THE ASTROPHYSICAL JOURNAL, 337:97–107, 1989 February 1


# THE EFFECTS OF MAGNETIC FIELDS ON THE GROWTH OF THERMAL INSTABILITIES IN COOLING FLOWS

LAURENCE P. DAVID
Harvard-Smithsonian Center for Astrophysics

AND

JOEL N. BREGMAN
NRAO[1]

*Received 1988 May 13; accepted 1988 July 13*

## ABSTRACT

We have examined the effects of heat conduction and magnetic fields on the growth of thermal instabilities in cooling flows using a time-dependent hydrodynamics code. We find that for magnetic fields strengths of $\approx 1$ $\mu$G (similar to that which may exist in intracluster gas), magnetic pressure forces can completely suppress shocks from forming in thermally unstable entropy perturbations with initial length scales as large as 20 kpc, even for initial amplitudes as great as 60%. The suppression of shock formation in cooling condensations significantly reduces the predicted luminosity of optical and ultraviolet emission lines produced as thermally unstable gas cools and decouples from a cooling flow. We find that perturbations with initial amplitudes of 50% and initial magnetic field strengths of 1 $\mu$G cool to $10^4$ K on a time scale which is only 22% of the initial instantaneous cooling time. Nonlinear perturbations can thus condense out of cooling flows on a time scale substantially less than the time required for linear perturbations and produce significant mass deposition of cold gas while the accreting intracluster gas is still at large radii. Our models with heat conduction indicate that in order for entropy perturbations to condense out of cooling flows the magnetic fields must be sufficiently tangled to reduce the Spitzer conductivity by a factor of $\sim 100$. We discuss some observational consequences of cooling condensations in cooling flows, in particular, the Faraday rotation that can be generated by cold, dense, high magnetic pressure clouds lying along the line of sight to cluster radio sources.

*Subject headings:* galaxies: intergalactic medium — galaxies: internal motions — hydromagnetics — magnetic fields — shock waves

## I. INTRODUCTION

The observed X-ray emission from early-type galaxies and clusters of galaxies is now commonly associated with thermal emission from hot gas (Forman and Jones 1982; Fabian, Nulsen, and Canizares 1984; Sarazin 1986). In some clusters of galaxies the estimated cooling time of the intracluster gas in the central regions of the cluster is less than a Hubble time. If heating is unable to balance cooling, the gas interior to a cooling radius (the radius at which the cooling time equals a Hubble time) will cool and accrete into the central galaxy in the cluster. Many reheating mechanisms have been proposed to prevent the intracluster gas from cooling, i.e., heating by galaxy motions (Miller 1986), heating by relativistic particles from an active galactic nucleus (Lea and Holman 1978; Tucker and Rosner 1983), supernovae (Silk *et al.* 1986), and heat conduction (Bertschinger and Meiksin 1986). None of these heating mechanisms, however, can simultaneously supply sufficient heating to balance radiative cooling, suppress the growth of entropy perturbations at all radii interior to a cooling radius, and reproduce the temperature gradient observed in some cluster cooling flows (Bregman and David 1988, 1989). If no heating mechanism can satisfy these three conditions, then nearly all of the X-ray emitting gas within a cooling radius will condense out of the cooling flow via thermal instabilities.

Since thermal instabilities are such an integral aspect of the cooling flow scenario we have undertaken a program to investigate observational consequences of thermally unstable perturbations in cooling flows. In David, Bregman, and Seab (1988, hereafter Paper I), we investigated the nonlinear growth of entropy perturbations in the absence of magnetic fields and heat conduction. We found that for conditions appropriate to cluster cooling flows, perturbations larger than $\approx 3$ kpc evolved through three stages: (1) an initial stage, with a duration of $\sim 50\%$–$60\%$ of the initial instantaneous cooling time, during which the central region in a perturbation cools and forms a cold ($T = 10^4$ K) dense core, (2) a supersonic accretion phase onto the cold core that is driven by the pressure gradient between the cold core and the ambient medium which lasts for $10^5$–$10^6$ yr and attains peak shock velocities of 80–120 km s$^{-1}$, and (3) a subsonic accretion phase that commences once gas above $\approx 5 \times 10^5$ K begins accreting onto the cold core. Perturbations smaller than $\approx 3$ kpc cool isobarically to low temperatures and do not generate sufficient pressure gradients to accelerate gas to supersonic velocities. The line emission produced during the supersonic accretion phase in large pertubations was found to be of a higher ionization level and a lower luminosity than the observed optical emission from cluster cooling flows (Hu, Cowie, and Wang 1985). This indicates that some other heating mechanism is responsible for producing the observed optical emission in cluster cooling flows (i.e., photoionization from newly formed stars or the diffuse X-ray emission).

Several investigators have found that some radio sources within high X-ray luminosity clusters have very large Faraday rotation measures (Kato *et al.* 1987; Dreher, Carilli, and Perley

[1] National Radio Astronomy Observatory is operated by the Associated Universities, Inc., under contract by the National Science Foundation.

1987). The observed Faraday rotation can be generated as the linearly polarized radio emission traverses the cluster if the intracluster gas has a magnetic field strength of $\sim 1$ $\mu$G (Dennison 1980; David *et al.* 1988) and is not too severely tangled. The presence of magnetic fields in the intracluster medium can have a significant effect on the dynamics of cooling gas (Soker and Sarazin 1988). As gas cools below $10^5$ K, the magnetic pressure within a perturbation can become comparable to the thermal gas pressure. In this paper we examine the influence of magnetic fields on the growth of thermal instabilities in cooling flows by including a magnetic pressure term and heat conduction in the hydrodynamics equations. We also discuss some of the observable consequences of cooling condensations.

We describe our numerical hydrodynamics method used to investigate the nonlinear growth of entropy perturbations in § II. The evolution of perturbations with various initial magnetic field strengths and heat conduction efficiencies is given in § III. In § IV we discuss the observability of cooling condensations in cooling flows.

## II. METHOD

The numerical technique used to investigate the nonlinear growth of thermal instabilities in hot ($T = 10^6$–$10^8$ K) gas was described in detail in Paper I. In this section we briefly review our procedure and describe the additional physics included in the present simulations.

All models begin with static gas at constant pressure with an entropy perturbation of the following form:

$$n(x) = n_0(1 + Ae^{-(x/s)^2}), \quad \text{(1a)}$$

$$T(x) = T_0(1 + Ae^{-(x/s)^2})^{-1}, \quad \text{(1b)}$$

where $n_0$ and $T_0$ are the initial density and temperature of the ambient gas, $A$ is the amplitude of the perturbation, and $s$ is the length scale of the perturbation. The plane-parallel, time-dependent, hydrodynamics equations (see eqs. [1]–[3] in Paper I) are then solved using a modified version of the SOLA-STAR hydrodynamics code described in Cloutman (1980) and Ruppel and Cloutman (1975). Since the above equations are symmetric, only half of the perturbation is modeled in the hydrodynamics code with the peak density occurring in the innermost cell. In order to obtain sufficient resolution in the inner regions of the perturbation, a logarithmic grid is used with the inner cell width equal to $10^{-3}$ s and the width of the entire grid equal to 10 s. All simulations are followed in Lagrangian space.

As gas cools below $10^6$ K, the recombination time of many ions becomes longer than the cooling time of the gas. At these lower temperatures the gas becomes over ionized with respect to the electron temperature and the actual cooling rate is less than the equilibrium value. Shocks can also lead to nonequilibrium effects if the electron temperature increases faster than the ionization temperature. In order to account for these nonequilibrium effects, we used tabulated values of a nonequilibrium radiative cooling function obtained from Edgar (1988), which is based on the assumption of isochoric cooling. The ionization state of the gas is followed separately using electron and H charge exchange recombination and ionization coefficients given in Edgar (1988). Hydrogen charge exchange recombination is the dominant recombination mechanism below $\approx 2 \times 10^4$ K, when the number density of neutral H is comparable to the number density of metals. The He charge exchange recombination rate is one order of magnitude less than hydrogen and is not included in these simulations. By carefully following the cooling and ionization of the gas we can determine the time scale for perturbations to condense out of cooling flows.

A comparison between our numerical integration scheme and the linear theory of Mathews and Bregman (1978) is shown in Figure 1 for a model with $n_0 = 10^{-2}$ cm$^{-3}$, $T_0 = 3 \times 10^7$ K, $A = 0.01$, and $s = 10$ kpc. Notice that our numerical result closely agrees with the linear theory until the amplitude of the perturbation reaches $\sim 5\%$. As the amplitude continues to increase, nonlinear effects become significant and the amplitude of the perturbation increases more rapidly than predicted by linear theory. The gas in the central region of the perturbation cools to $10^4$ K in 60% of the initial instantaneous cooling time in this model. Initially unperturbed gas would cool to $10^4$ K in 65% of the initial instantaneous cooling time.

The origin of the magnetic fields in intracluster gas is uncertain, but there is some evidence for its existence from Faraday rotation measures of cluster radio sources (Kato *et al.* 1987; Dreher, Carilli, and Perley 1987). We allow for the presence of a magnetic field in our simulations by including a magnetic pressure term in the equation of motion ($P_B = B^2/8\pi$). The magnetic pressure is unlikely to be comparable to the thermal pressure in the ambient hot gas, since this would require $B \sim 10^{-4}$ G and lead to uniformly large rotation measures or depolarization effects in radio sources, which is not commonly observed. However, as the gas within a perturbation cools, the component of the $B$ field perpendicular to the direction of compression increases ($B \propto \rho$ in plane-parallel symmetry). Magnetic pressure forces will begin to dominate the gas dynamics before the gas cools to $10^4$ K for initial magnetic fields as weak as 0.03 $\mu$G. Compression of the perturbation ceases once the magnetic pressure balances the thermal gas pressure of the ambient medium. In § III we present a series of models with a range of values for the ratio of the initial magnetic pressure to the initial thermal pressure $\beta = P_B(t = 0)/P_g(t = 0)$.

The effect of heat conduction on thermal instabilities is very sensitive to the topology of the magnetic field in cooling flows. The role of conduction is analyzed in this paper by including the term $\nabla \cdot \boldsymbol{q}$ on the right-hand side of the energy equation given in Paper I, where $q$ is the heat flux defined as $q = \mu\kappa\, dT/dr$. The Spitzer (1978) conductivity $\kappa$, is reduced by a factor $0 < \mu < 1$, which corresponds to the degree of tangling in the magnetic field. The growth of thermal instabilities with heat conduction will be presented in § III with a range of values of $\mu$. We also compare our numerical results with the linear theory of Field (1968).

## III. RESULTS

### a) *Magnetic Pressure Effects*

In Paper I we analyzed the growth of thermal instabilities in the absence of magnetic fields. We found that in conditions appropriate for cluster cooling flows ($T_0 \approx 3 \times 10^7$ K, $n_0 \approx 10^{-2}$ cm$^{-3}$), only perturbations with an initial length scale greater than 3 kpc and an initial amplitude greater than 1% developed shocks after cooling; the central density in these perturbations increased by a factor of $\approx 1000$. Any magnetic fields entrained within a perturbation can thus be amplified by up to a factor of 1000 as the gas cools, which corresponds to an increase in $P_B$ by a factor of $10^6$. If the magnetic pressure

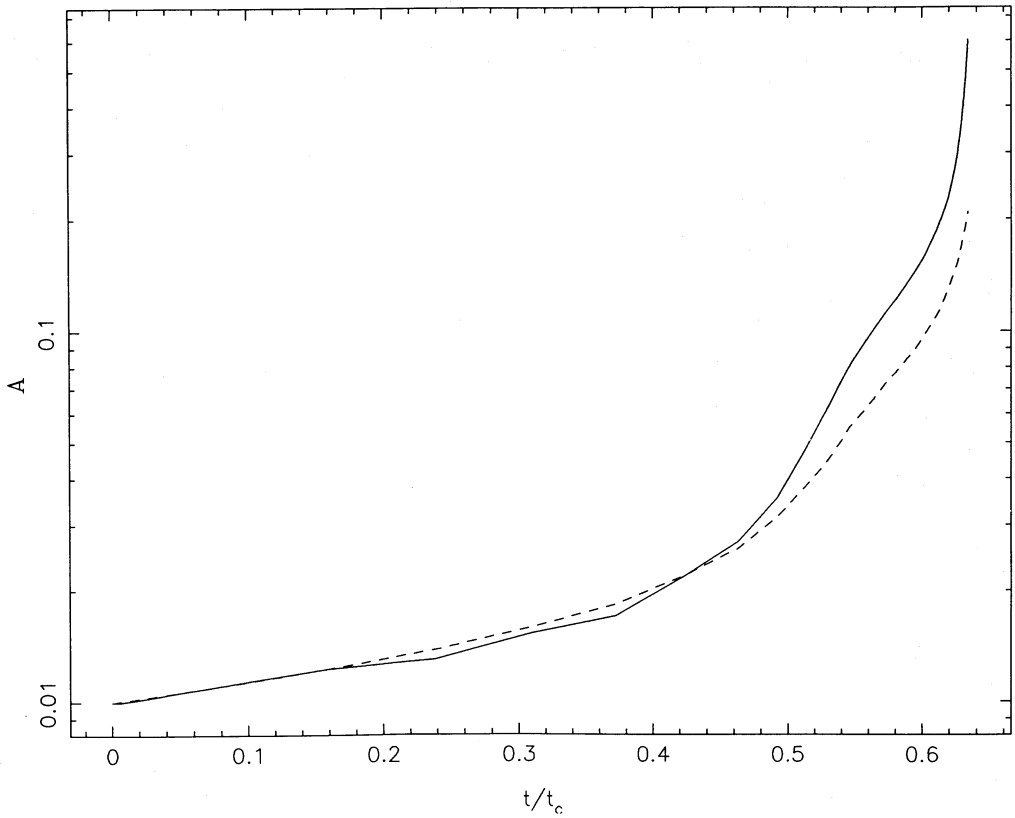


FIG. 1.—The growth of an entropy perturbation with $n_0 = 10^{-2}$ cm$^{-3}$, $T_0 = 3 \times 10^7$ K, and $A = 0.01$. Our numerical results are indicated by the solid line. Dashed curve illustrates the growth rate given by the linear theory of Mathews and Bregman (1978). The horizontal axis is in units of the initial instantaneous cooling time.

increases to the point where it can balance the gas pressure of the ambient medium then compression of the instability ceases and the central density remains constant as the gas continues to cool. Assuming isobaric cooling, this occurs at a temperature given by $T_1^2 = (\frac{5}{6})(v_A/c_a)^2 T_0^2$, where $v_A$ and $c_a$ are the Alfven velocity and adiabatic sound speed of the initially unperturbed gas. In order for shock formation to be completely suppressed, the magnetic pressure in the central regions of the perturbation must exceed the ambient gas pressure soon after the thermal instability begins to cool isochorically. At this time the Alfvén velocity becomes greater than the adiabatic sound speed and the Alfvén Mach number of the perturbed gas remains less than one.

We have investigated the behavior of thermal instabilities for a range of magnetic pressures and perturbation amplitudes ($\beta$ and $A$; Table 1). All the models have the same initial density, temperature, and length scale as model C of Paper I ($n_0 = 10^{-2}$ cm$^{-3}$, $T_0 = 3 \times 10^7$ K, $s = 10$ kpc). The initial instantaneous cooling time [$t_c = 3kT/(2n\Lambda)$, where $\Lambda$ is the radiative cooling coefficient] is $2 \times 10^9$ yr in these models. Models with smaller values of $\beta$ have also been computed, but we do not label these models individually since they evolve identically to the models described in Paper I. All models with magnetic fields evolve through three distinct evolutionary sequences depending on the initial magnetic field strength. There are three ranges of interest in the initial magnetic field strength. In models with $\beta \lesssim 3 \times 10^{-7}$ ($B_0 \lesssim 0.02$ $\mu$G) and $A = 0.1$ the magnetic pressure never becomes comparable to the gas pressure anywhere in the perturbation. The perturbation is compressed by the maximum amount in these models and the final magnetic field strength $B_f$ is $1000B_0$. For $3 \times 10^{-7} \lesssim \beta \lesssim 5 \times 10^{-4}$ ($0.02 \lesssim B_0 \lesssim 0.7$ $\mu$G) the magnetic pressure eventually dominates over the gas pressure, but not until the central gas has cooled to below $\approx 10^5$ K and shocks still develop. In models with $\beta \lesssim 5 \times 10^{-4}$ ($B \gtrsim 0.7$ $\mu$G) shocks are completely suppressed, even in perturbations with initial amplitudes as great as 60% (see Table 1). For initial magnetic fields strengths above 0.02 $\mu$G, the magnetic pressure remains constant once pressure balance with the ambient gas pressure is attained and $B_f$ remains a constant value of $\approx 30$ $\mu$G. The central temperature in a perturbation only decreases by an order of magnitude during the first 99% of the integrated cooling time $t_1$ (the time required for the central region of a perturbation to completely cool to $10^4$ K). Since magnetic fields do not become dynamically important until much lower temperatures have been reached, they have little effect on the time required for complete cooling (Table 1).

The peak shock velocity $v_s$ and peak shock strength $M_s$ decrease rapidly with increasing $\beta$ in models that develop shocks ($B_0 \lesssim 0.7$ $\mu$G; see Table 1). Even a relatively weak initial magnetic field strength of 0.3 $\mu$G reduces the peak shock strength by 38% relative to the case without a magnetic field (model C of Paper I). A comparison between the evolution of the temperature profiles of models A, B, and D is shown in Figure 2. These figures show the temperature profile in a perturbation at several different stages. Because of the large difference in cooling times between gas slightly above $10^4$ K and gas at $10^7$ K, the initially unperturbed region does not evolve sig-

TABLE 1

THERMAL INSTABILITY MODELS WITH MAGNETIC PRESSURE

| Model | $A$[a] | $\beta$[b] | $B_0$[c] ($\mu$G) | $B_f$[d] ($\mu$G) | $t_1/t_c$[e] | $\rho_f/\rho_i$[f] | $v_s$[g] (km s$^{-1}$) | $M_s$[h] | $x_{sf}$[i] (pc) | $x_{se}$[j] (pc) | $t_{sh}$[k] ($10^5$ yr) | $T_{sh}$[l] ($10^5$ K) | $f_c$[m] (%) | $f_{sh}$[n] (%) |
|---|---|---|---|---|---|---|---|---|---|---|---|---|---|---|
| A..... | 0.1 | $10^{-5}$ | 0.10 | 28.5 | 0.51 | 224. | 110. | 2.7 | 0.92 | 13.5 | 1.4 | 1.2 | 0.9 | 2.9 |
| B..... | 0.1 | $10^{-4}$ | 0.32 | 23.5 | 0.51 | 50.9 | 85.2 | 1.9 | 3.62 | 11.7 | 1.5 | 1.5 | 1.7 | 1.6 |
| C..... | 0.1 | $5 \times 10^{-4}$ | 0.71 | 27.4 | 0.51 | 27.8 | 71.3 | 1.2 | 11.3 | 14.7 | 0.6 | 2.7 | 2.4 | 1.1 |
| D..... | 0.1 | $10^{-3}$ | 1.0 | 30.2 | 0.51 | 18.2 | ... | ... | ... | ... | ... | ... | ... | ... |
| E..... | 0.2 | $10^{-3}$ | 1.0 | 34.0 | 0.41 | 22.1 | ... | ... | ... | ... | ... | ... | ... | ... |
| F..... | 0.4 | $10^{-3}$ | 1.0 | 40.0 | 0.27 | 26.3 | ... | ... | ... | ... | ... | ... | ... | ... |
| G..... | 0.5 | $10^{-3}$ | 1.0 | 41.1 | 0.22 | 26.9 | ... | ... | ... | ... | ... | ... | ... | ... |
| H..... | 0.6 | $10^{-3}$ | 1.0 | 42.7 | 0.18 | 27.9 | ... | ... | ... | ... | ... | ... | ... | ... |

NOTE.—All models begin with $n_0 = 10^{-2}$ cm$^{-3}$, $T_0 = 3 \times 10^7$ K, and $s = 10$ kpc. For comparison models with $A = 0.0$ have $t_1/t_c = 0.655$.

[a] Initial amplitude $A$.
[b] Initial ratio of magnetic pressure to thermal pressure $\beta$.
[c] Initial magnetic field strength $B_0$.
[d] Final magnetic field strength $B_f$.
[e] Integrated cooling time $t_1$, initial instantaneous cooling time $t_c$.
[f] Compression ratio $\rho_f/\rho_i$.
[g] Peak shock velocity $v_s$.
[h] Peak shock strength $M_s$.
[i] Shock formation radius $x_{sf}$.
[j] Shock dissipation radius $x_{se}$.
[k] Shock life time $t_{sh}$.
[l] Average preshock gas temperature $T_{sh}$.
[m] Fraction of gas within the cold core $f_c$.
[n] Fraction of gas which accretes onto the cold core supersonically $f_{sh}$.

nificantly after the core develops. The accretion shock is easily identifiable in this figure as a sharp spike in the temperature profile located between the stationary cold core and the infalling hot ambient medium. The decrease of the shock strength with increasing $\beta$ is apparent in these figures. Also notice that the location where the shock forms $x_{sf}$ increases with increasing $\beta$, corresponding to an increase in the fraction of gas contained within the cold core $f_c$ (see Table 1). The duration of the shock $t_{sh}$ and the fraction of gas that accretes onto the cold score supersonically $f_{sh}$ both decrease with increasing $\beta$, while the average temperature of the preshocked gas $T_{sh}$ increases with $\beta$ (Table 1). There is little difference between the density evolution in models A, B, and D until the magnetic pressure becomes significant (compare the first three density profiles in Figures 3*a*–3*c*). Since model D has the highest value of $\beta$, the magnetic pressure is able to balance the ambient thermal pressure at a higher temperature than in models A and B and produce the least compression ratio $\rho_f/\rho_i$ (Table 1). The final density in thecold core in model D is decreased by a factor of 100 compared to the case without a magnetic field, but the cold core in model D contains 3 times the mass due to the increase in $x_{sf}$.

The evolution of $P_B$ and $P_g$ for model D is shown in Figure 4. The final balance between $P_B$ in the center of the perturbation and $P_g$ of the ambient medium is illustrated in this figure. There is still a small gradient in the total pressure at the interface of the cold core and the ambient medium but it is not strong enough to accelerate gas to supersonic velocities and produce an accretion shock. Models with smaller values of $B_0$ develop steeper gradients of total pressure. The final total presure is $\approx \frac{1}{3}$ of the initial total pressure due to radiative cooling of the ambient gas.

In Paper I we confined our investigation to models with $A \leq 0.1$. The integrated cooling time was $\approx \frac{1}{2}$ of the initial instantaneous cooling time in all of these models. For comparison, initially unperturbed gas cooled to $10^4$ K in 65% of the initial instantaneous cooling time. While the integrated cooling time of a perturbation does not vary significantly in models with $A \lesssim 0.1$ (see Paper I), there is a significant reduction in the integrated cooling time for stronger perturbations (compare the results of models E, F, G, and H in Table 1). For a 60% perturbation the integrated cooling time is only 18% of the initial instantaneous cooling time, and only 28% of the time required for initially unperturbed gas to cool completely. Both the final magnetic field strength and the final density are directly correlated to the initial amplitude of the perturbation (Table 1). This is due to the fact that the central gas cools more rapidly in models with stronger perturbations so that the gas pressure at the outer boundary does not decrease as significantly before the core completely cools and a higher central magnetic pressure is required to halt compression (see Table 1).

### b) *Effects of Heat Conduction*

An energy transport mechanism that may affect the development of thermal instabilities in cooling flows is heat conduction. Heat conduction will completely suppress the growth of a perturbation if the rate of energy transport into a perturbation is greater than the radiative loss rate. Since the total radiative cooling rate is proportional to the volume of a perturbation and the total heat flux into a perturbation is proportional to the area of the perturbation, heat conduction only suppresses the growth of perturbations less than a critical length scale $s_{crit}$. The balance between heat conduction and radiative cooling is inherently unstable. Perturbations slightly larger than $s_{crit}$ continue to grow while perturbations slightly smaller than $s_{crit}$ are completely suppressed. Field (1965) derived an expression for $s_{crit}$ in terms of the temperature and density of a perturbation by assuming full Spitzer conductivity and using linear perturbation techniques. This condition can be inverted to determine the fraction of full Spitzer conductivity, denoted by $\mu$, required

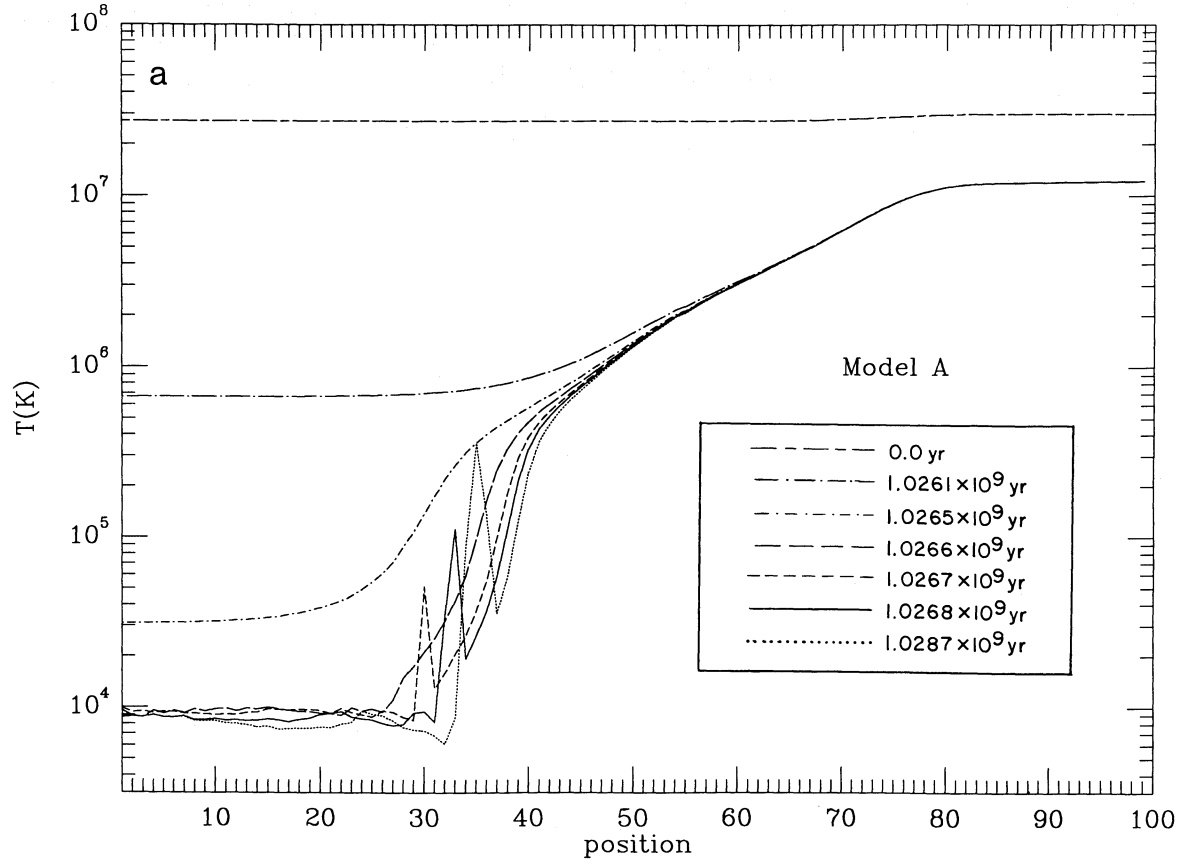


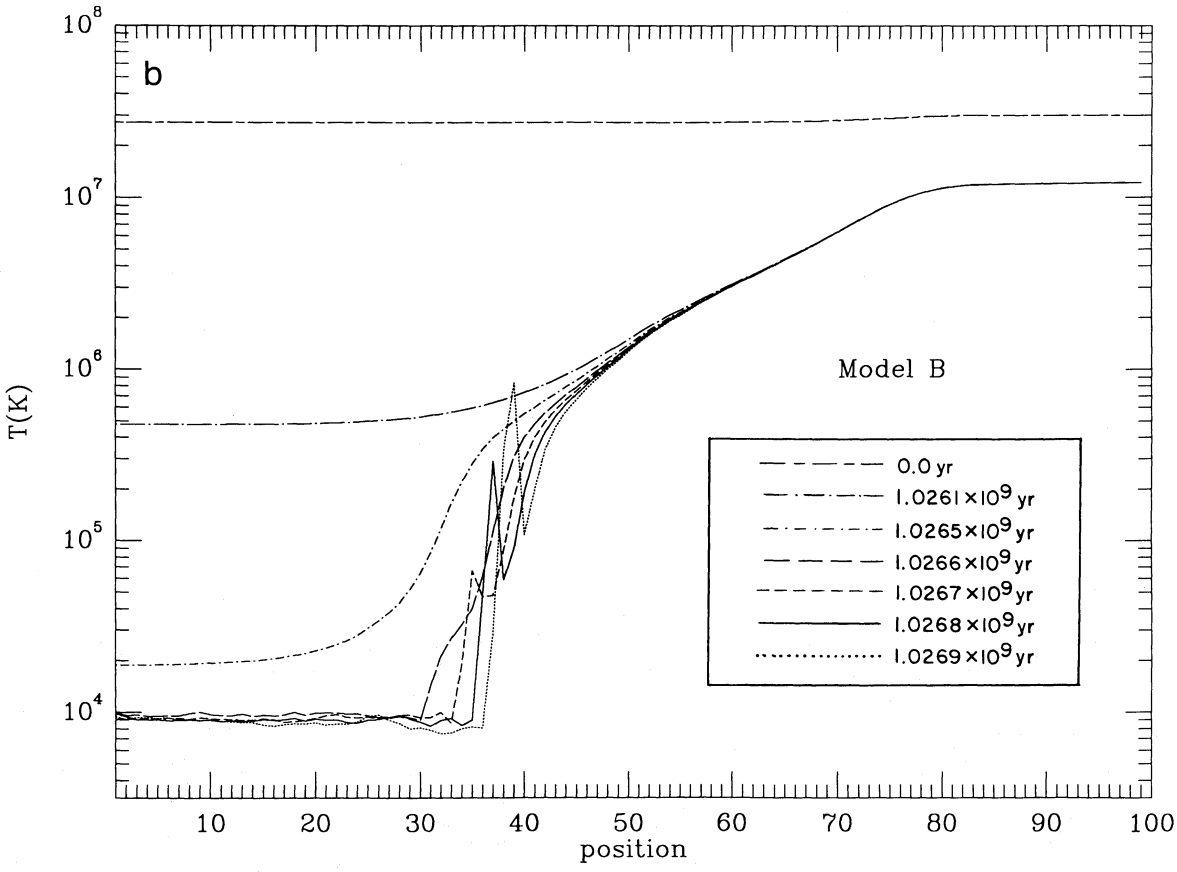


FIG. 2.—(*a*)–(*c*) Temperature profiles for models A, B, and D at several different times. The sharp spike in the temperature profiles correspond to the location of the accretion shock. The horizontal axis corresponds to the cell number in the hydrodynamics code. For comparison, cell 50 is initially located at 1 kpc, cell 75 at 10 kpc, and cell 100 at 100 kpc.

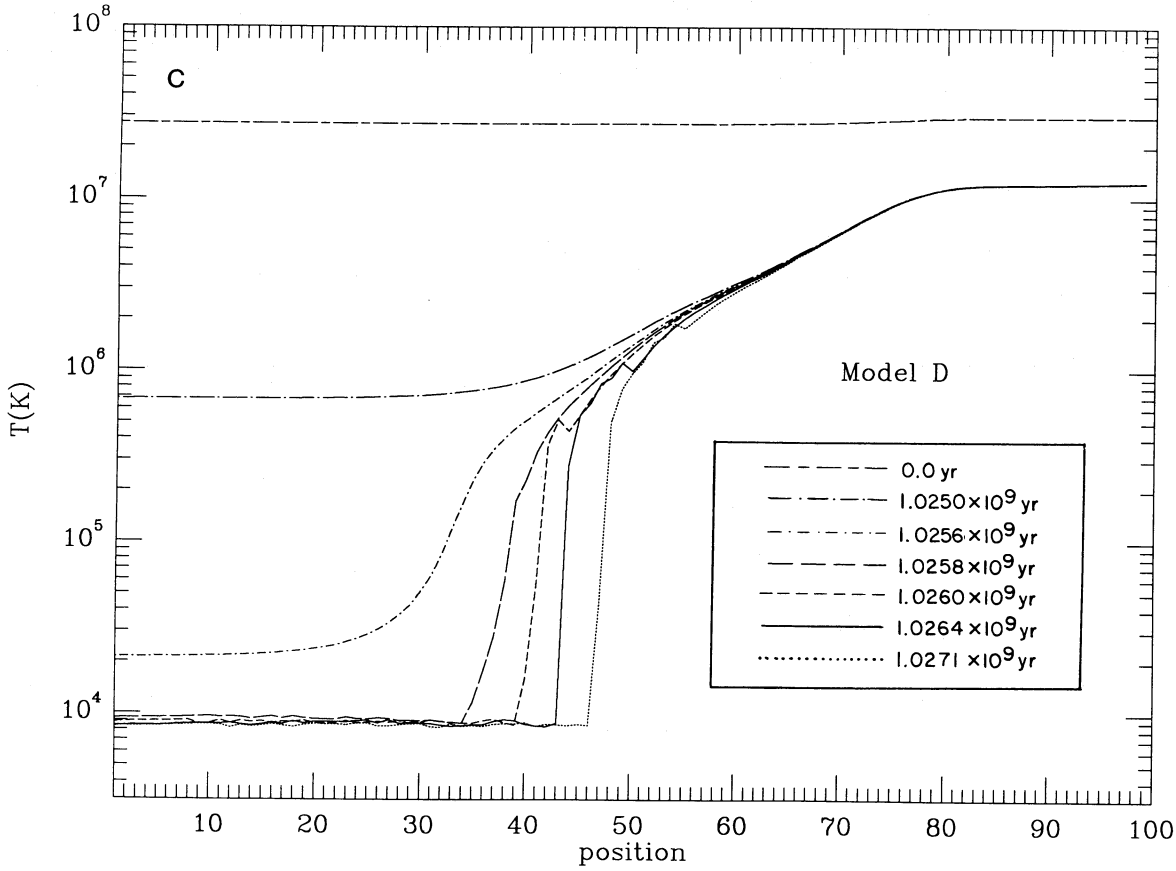


FIG. 2—*Continued*

to suppress the growth of a thermal instability of length scale $s$

$$\mu_{\rm crit} = (3.8 \times 10^{-3})\left(\frac{s}{10\ {\rm kpc}}\right)^2\left(\frac{T_0}{3 \times 10^7\ {\rm K}}\right)^{-7/2} \times \left(\frac{n_0}{0.01\ {\rm cm}^{-3}}\right)^2\left(\frac{\Lambda}{2 \times 10^{-23}\ {\rm ergs\ cm^3\ s^{-1}}}\right). \quad (2)$$

To determine whether nonlinear effects significantly alter the linear theory of Field (1968), we computed a series of models with $T_0 = 3 \times 10^7$ K, $n_0 = 10^{-2}$ cm$^{-3}$, s = 10 kpc, $A = 0.01$, and a range of values of $\mu$. The amplitude evolution of these models is illustrated in Figure 5. Our numerical results indicate that the critical Spitzer conduction coefficient required to suppress the growth of this model is $\approx 5 \times 10^{-3}$, which is in good agreement with the linear theory. A model with the exact value of $\mu_{\rm crit}$ would maintain its initial amplitude and correspond to a horizontal line in Figure 5. Since this is an unstable equilibrium configuration, all of the models shown in Figure 5 are either damped or continue to grow.

To determine the sensitivity of $\mu_{\rm crit}$ to the amplitude of a perturbation, a series of models were examined with larger amplitude ($A = 0.1$), a range of values for $\mu$, but otherwise the same initial parameters as the above models. Even with an order of magnitude increase in $A$, we find that $\mu_{\rm crit} \approx 10^{-2}$ (see Table 2) which is only a factor of 2 increase over the linear theory. In models with $A = 0.1$ and $\mu > 10^{-3}$, shock formation is completely suppressed. Since heat conduction is the most significant at high temperatures, a small amount of heat conduction significantly increases the integrated cooling time and decreases the compression ratio (see Table 2). Heat conduction is very inefficient in models with $\mu < 10^{-3}$, and shocks still develop. Heat conduction never becomes saturated in any of these models, even those that develop steep temperature gradients and shocks. The peak shock velocity, shock strength, shock lifetime, and fraction of gas that accretes onto the cold core supersonically all increase with decreasing $\mu$ (see Table 2). The results of model C in Paper I are shown in Table 2 for comparison. It is obvious from Table 2 that the shocks produced by thermal instabilities in cooling flows can be weakened significantly by heat conduction even if the magnetic field lines are severely tangled.

## IV. DISCUSSION AND SUMMARY

### *a) Growth Rate of Thermal Instabilities*

If cluster cooling flows exist, then nearly all of the hot X-ray emitting gas must condense out of the flow before accreting into the nucleus of the central dominant galaxy. This is likely to occur if the gas is subjected to nonlinear entropy perturbations throughout the cooling region. Strong perturbations can condense out of a cooling flow on a time scale significantly less than the intantaneous cooling time and produce significant mass deposition of cold gas at large radii. From our numerical simulations, we find that entropy perturbations with initial amplitudes between 10%–60% cool to $10^4$ K in 51%–18% of the initial instantaneous cooling time of the unperturbed gas. Linear entropy perturbations grow too slowly and may even

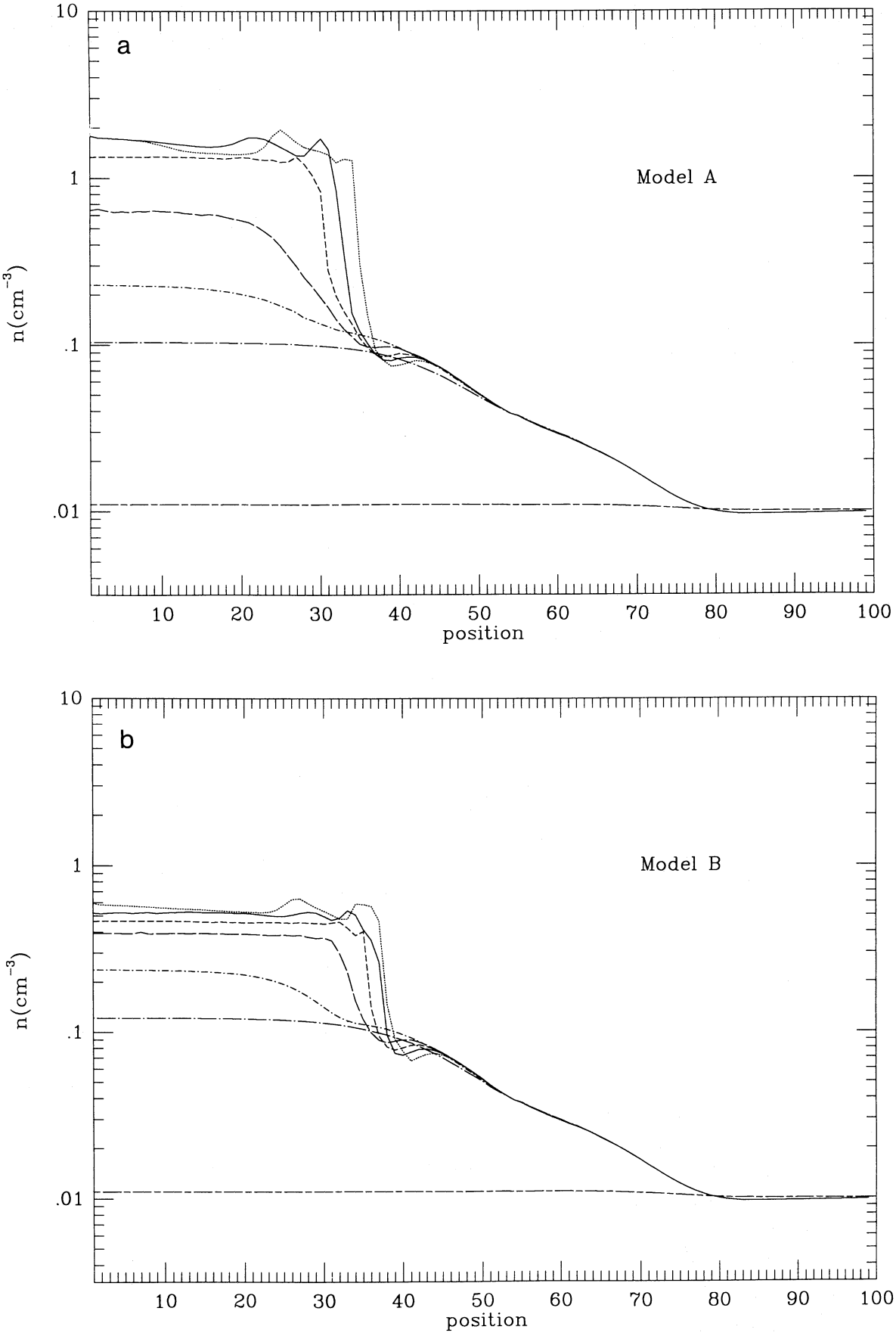


FIG. 3.—(*a*)–(*c*) Density profiles for models A, B, and D at the same times as given in Fig. 2

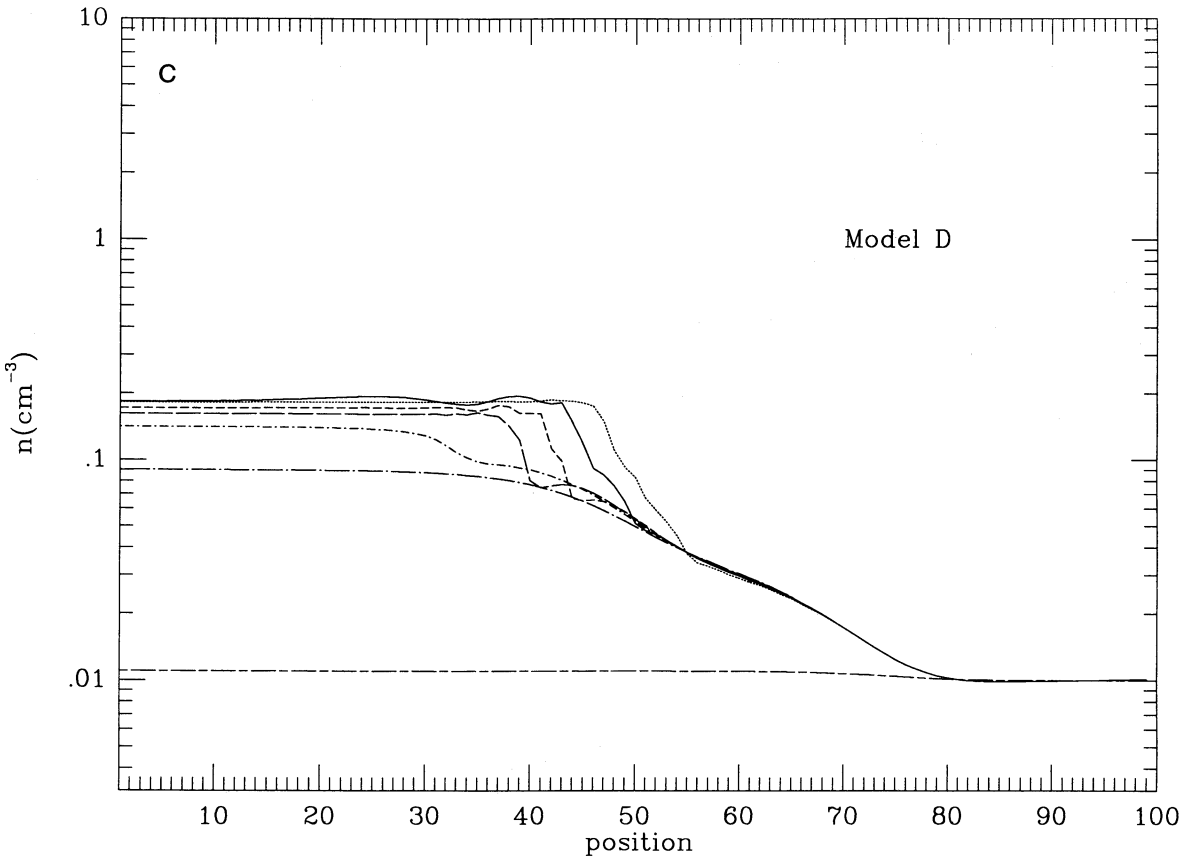


FIG. 3—*Continued*

be stable due to the effects of buoyancy (Balbus 1988). Fabian, Arnaud, and Thomas (1987) have shown that to accurately fit the observed *Einstein* IPC radial profiles of clusters, the mass accretion rate of the hot X-ray emitting gas must decrease with decreasing radius interior to the cooling radius. If mass deposition did not occur within the cooling radius, the X-ray surface brightness profiles of clusters would be more strongly peaked toward the center of a cluster than is observed (Sarazin 1987).

There are many nonlinear effects operating in galaxy clusters that can produce strong perturbations. One mechanism for producing the required nonlinear entropy perturbations in cluster cooling flows is through ram pressure stripping of galaxies. As galaxies pass through the cluster core, the cooler gas within the interstellar medium of the galaxy is deposited in the wake of the galaxy (Gaetz, Salpeter, and Shaviv 1987). The injected cold gas within galactic wakes can thus provide the

TABLE 2

THERMAL INSTABILITY MODELS WITH HEAT CONDUCTION

| $\mu$[a] | $t_1/t_c$[b] | $\rho_f/\rho_i$[c] | $v_s$[d] (km s$^{-1}$) | $M_s$[e] | $x_{sf}$[f] (pc) | $x_{se}$[g] (pc) | $t_{sh}$[h] ($10^5$ yr) | $T_{sh}$[i] ($10^5$ K) | $f_c$[j] (%) | $f_{sh}$[k] (%) |
|---|---|---|---|---|---|---|---|---|---|---|
| $8 \times 10^{-3}$ ..... | 0.81 | 4.52 | ... | ... | ... | ... | ... | ... | ... | ... |
| $4 \times 10^{-3}$ ..... | 0.76 | 27.5 | ... | ... | ... | ... | ... | ... | ... | ... |
| $10^{-3}$ ..... | 0.68 | 97.6 | ... | ... | ... | ... | ... | ... | ... | ... |
| $5 \times 10^{-4}$ ..... | 0.67 | 304. | 32.1 | 1.2 | 3.26 | 4.73 | 0.75 | 2.0 | 2.4 | 1.1 |
| $10^{-4}$ ..... | 0.64 | 862. | 57.9 | 1.8 | 2.71 | 5.71 | 0.92 | 1.2 | 1.8 | 1.6 |
| 0.0 ..... | 0.51 | 1530 | 136. | 3.2 | 0.21 | 6.89 | 1.60 | 8.0 | 1.0 | 5.0 |

NOTE.—All models begin with $n_0 = 10^{-2}$ cm$^{-3}$, $T = 3 \times 10^7$ K, $A = 0.10$, and $s = 10$ kpc.
[a] The reduction coefficient of heat conduction $\mu$.
[b] Integrated cooling time $t_1$, initial instantaneous cooling time $t_c$.
[c] Compression ratio $\rho_f/\rho_i$.
[d] Peak shock velocity $v_s$.
[e] Peak shock strength $M_s$.
[f] Shock formation radius $x_{sf}$.
[g] Shock dissipation radius $x_{se}$.
[h] Shock life time $t_{sh}$.
[i] Average preshock gas temperature $T_{sh}$.
[j] Fraction of gas within the cold core $f_c$.
[k] Fraction of gas which accretes onto the cold core supersonically $f_{sh}$.

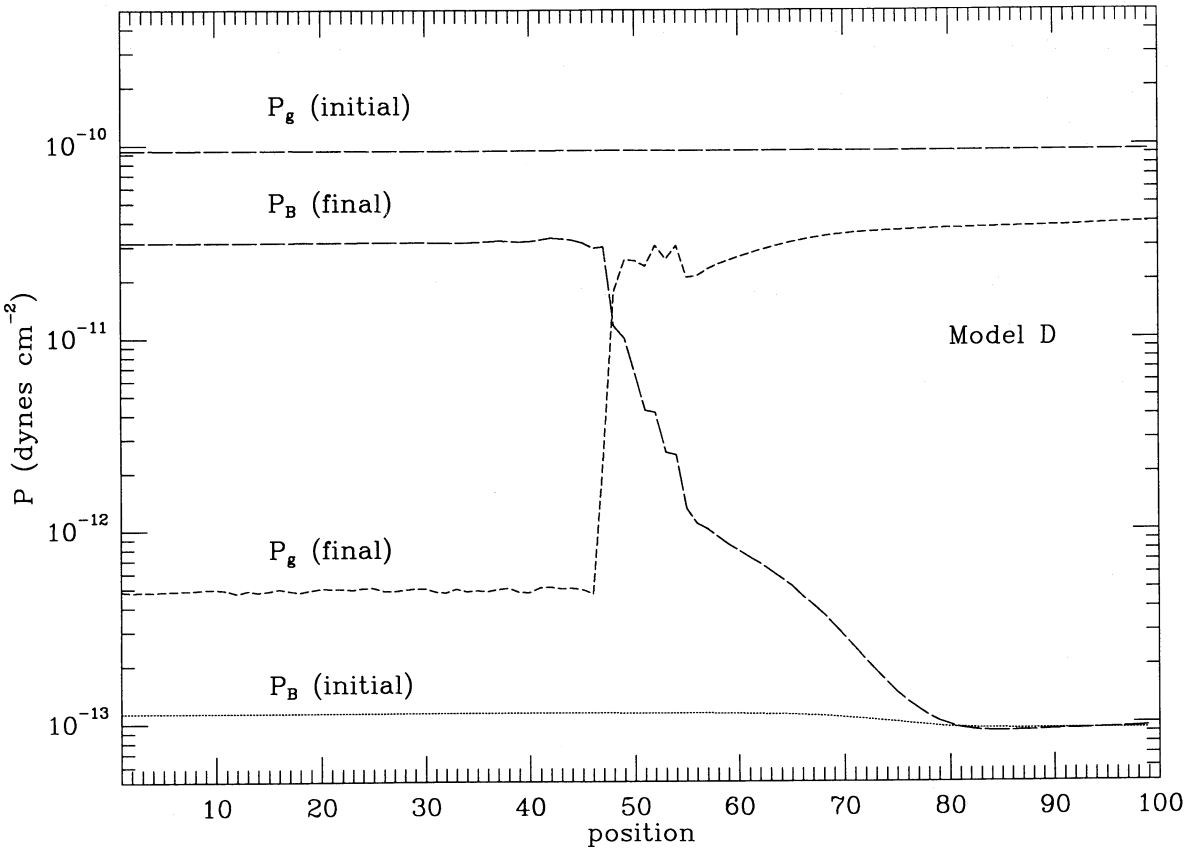


FIG. 4.—The initial and final magnetic ($P_B$) and thermal ($P_g$) pressures in model D. The time at the end of the run is $1.0271 \times 10^9$ yr. Notice that the total pressure $P_B + P_g$ is roughly a constant at the end of the run.

necessary seed onto which the hotter intracluster medium can condense provided the ejected gas from the galaxy is larger than $s_{crit}$.

### b) *Detectability of Cooling Gas*

In Paper I we showed that most of the line emission produced by thermally unstable condensations in cooling flows occurred during the supersonic accretion phase. This emission was of a highly ionized nature, containing many strong ultraviolet lines, due to the nonequilibrium ionization of the accreting gas. However, models with magnetic field strengths similar to those that may exist in clusters prevent shocks from forming and render the ultraviolet lines unobservable. The initial thermal energy of the gas that was radiated away in our previous models during the supersonic accretion phase is transferred to the energy of the magnetic field as the gas is compressed.

The amount of gas with temperatures between $10^4$–$10^6$ K within a cooling radius is a fundamental test of the cooling flow hypothesis. Observed O VIII emission from M87 (Canizares *et al.* 1982) indicates the presence of gas with a temperature of $\approx 2 \times 10^6$ K. Optical emission, indicative of $10^4$ K gas, has been observed in many clusters with cooling flows (Hu, Cowie, and Wang 1985). At present, however, there is no data on the amount of gas at intermediate temperatures. *IUE* observations of A1795 and NGC 1275 (Norgaard-Nielsen, Jorgensen, and Hansen 1984; Fabian, Nulsen, and Arnaud 1984) have only been able to place upper limits on C IV $\lambda\lambda$1548, 1551 emission, which is a good spectral diagnostic for the presence of $10^5$ K gas. In Paper I, the C IV emission produced during the supersonic accretion phase was shown to be within one order of magnitude of the limits attainable by the *IUE*. Our current models with magnetic fields reduce the ultraviolet line strength significantly below the sensitivity of the *IUE*.

All of the models presented in this paper use plane-parallel symmetry. During the collapse of a purely spherical perturbation $B_0 \propto \rho^{2/3}$ and $P_B \propto \rho^{4/3}$. The critical magnetic field strength required to suppress shock formation in the models presented here would thus increase from 0.7 $\mu$G to $\sim 1.0$ $\mu$G if we used spherical symmetry. In realistic three-dimensional perturbations, it is likely that the collapse will proceed more rapidly in one direction (most likely in the direction perpendicular to the magnetic field lines since heat conduction is the most severely suppressed in this direction) and lead to sheets or filaments of cold gas. In such situations plane-parallel simulations are the most appropriate.

Since magnetic fields significantly decrease the line emission from cooling gas, one may be forced to use more indirect means to search for intermediate temperature gas in cooling flows. One possibility is through Faraday rotation measurements of radio sources within or behind clusters with cooling flows. Only a handful of radio galaxies are known to have rotation measures $R_m \gtrsim 500$ rad $m^{-2}$ (Kato *et al.* 1987). Two of these sources, Hydra A and Cygnus A, are the central dominant galaxy in clusters with high X-ray luminosities. Faraday

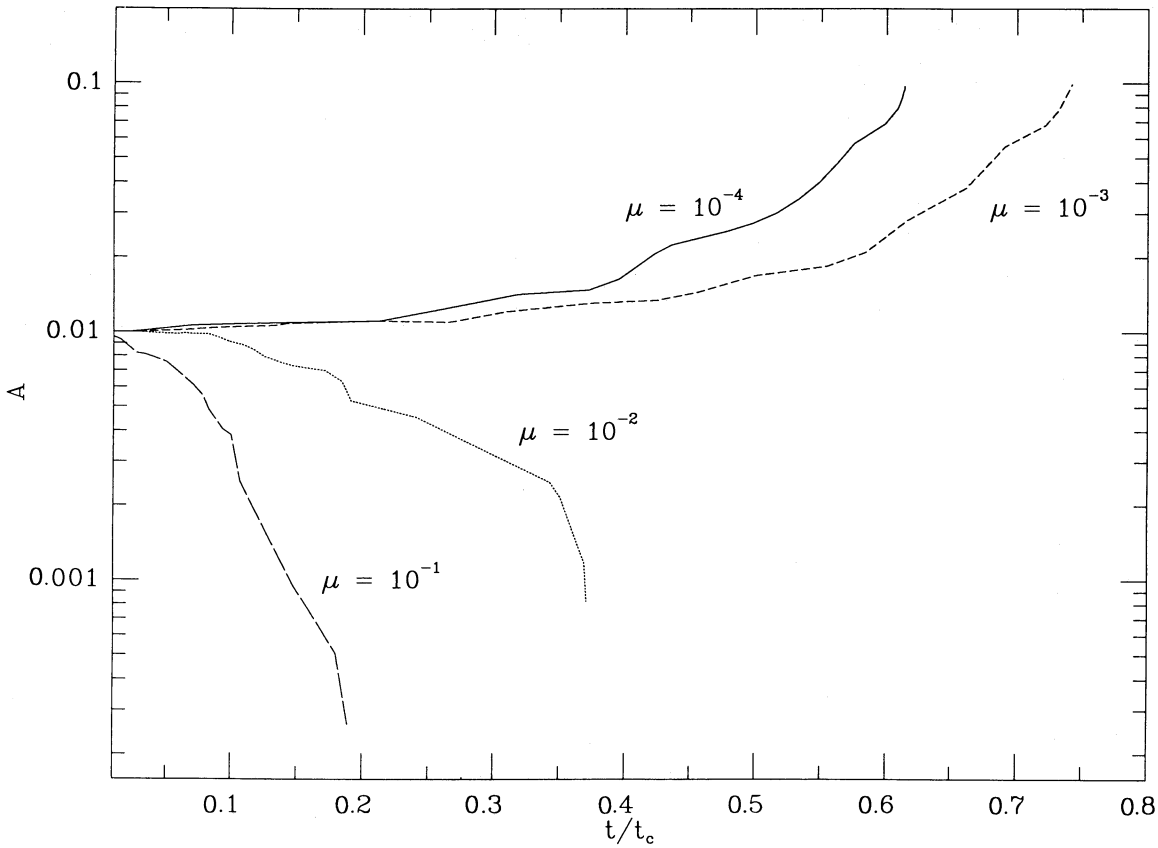


FIG. 5.—The growth of an entropy perturbation ($n_0 = 10^{-2}$ cm$^{-3}$, $T_0 = 3 \times 10^7$ K, and $A = 0.01$) with different reduction coefficients $\mu$ of heat conduction. The horizontal axis is the time in units of the initial instantaneous cooling time.

rotation measures the net magnetic field strength along the line of sight to a radio source. In order for the intracluster medium to produce a large rotation measure the magnetic field must be very strong or fairly uniform. Assuming constant electron number density $n_e$ in the intracluster gas (justified interior to a gas core radius) along the line of sight $L$ to a radio source, the Faraday rotation measure can be written as (David *et al.* 1988):

$$R_m = 812 m^{-2} \left(\frac{n_e}{10^{-2}\ \mathrm{cm}^{-3}}\right)\left(\frac{B_\parallel}{1\ \mu\mathrm{G}}\right)\left(\frac{L}{100\ \mathrm{kpc}}\right). \quad (6)$$

From this expression it is evident that the intracluster medium can only produce rotation measures greater than 500 rad $m^{-2}$ if the magnetic field is uniform over scales of close to 100 kpc, which is a typical cooling radius. As gas cools and accretes into the central dominate galaxy, the coupled magnetic field lines will be convected inward and may produce the required radial field lines. It is also possible that large rotation measures can be produced as linearly polarized radio emission propagates through small dense high magnetic field condensations. Using the final magnetic field strength and gas density in model D, the Faraday rotation measure per unit length through the condensation is 4.5 rad $m^{-2}$ pc$^{-1}$. This value corresponds to the rotation measure that would be produced in a cold condensation if the magnetic field was radial and the initial perturbation was transverse. A total path length of only 100 pc through such cold, dense, highly magnetized condensations is necessary to produce Faraday rotation measures of $\approx 500$ rad $m^{-2}$. This can occur if a single large 100 pc condensation or many small condensations lie along the line of sight to the radio source within a cooling radius. It is unlikely that many small condensations would have similarly oriented magnetic fields. It is much more likely that the observed Faraday rotation is due to single sheets or filaments of cold, high magnetic field condensations. Rotation measurements with spatial resolution of less than $\sim 100$ pc are required to determine whether the Faraday rotation of cluster radio sources is due to the extended intracluster medium of cooling condensations.

We would like to acknowledge many helpful conversations with Steve Balbus, Bill Forman, Craig Sarazin, and Noam Soker. We also appreciate Keith Arnaud and Harvey Tananbaum for carefully reading an earlier draft of this paper. This research was supported by NASA grant NAS8-30751.

REFERENCES

Balbus, S. A. 1986, *Ap. J.* (*Letters*), **303**, L79.
———. 1988, *Ap. J.*, **328**, 395.
Bertschinger, E., and Meiksin, A. 1986, *Ap. J.*, **306**, L1
Bregman, J. N., and David, L. P. 1988*a*, *Ap. J.*, **326**, 439.
Bregman, J. N., and David, L. P. 1989, *Ap. J.*, submitted
Canizares, C. R., Clark, G. W., Jernigan, J. G., and Markert, T. H. 1982, *Ap. J.*, **262**, 33.
Cloutman, L. D. 1980, Los Alamos Nat. Lab. Rept., LA-8452-MS.

David, L. P., Arnaud, K. A., Forman, W., and Jones, C. 1988, preprint.
David, L. P., Bregman, J. N., and Seab, C. G. 1988, *Ap. J.*, **329**, 66 (Paper I).
Dennison, B. 1980, *Ap. J.*, **236**, 761.
Dreher, J. W., Carilli, C. L., and Perley, R. A. 1987, *Ap. J.*, **316**, 611.
Edgar, R. J. 1988, private communication.
Fabian, A. C., Arnaud, K. A., and Thomas, P. A. 1987, in *Dark Matter in the Universe*, ed. J. Kormandy and G. P. Knapp (Dordrecht: Reidel), p. 201.
Fabian, A. C., Nulsen, P. E. J., and Arnaud, K. A. 1984, *M.N.R.A.S.*, **208**, 179.
Fabian, A. C., Nulsen, P. E. J., and Canizares, C. R. 1984, *Nature*, **310**, 733.
Field, G. B. 1965, *Ap. J.*, **142**, 531.
Forman, W., and Jones, C. 1982, *Ann. Rev. Astr. Ap.*, **20**, 547.
Gaetz, T. J., Salpeter, E. E., and Shaviv, G. 1987, *Ap. J.*, **316**, 530.
Hu, E. M., Cowie, L. L., and Wang, Z. 1985, *Ap. J. Suppl.*, **59**, 447.
Kato, T., Tabara, H., Inoue, M., and Aizu, K. 1987, *Nature*, **329**, 223.
Lea, S. M., and Holman, G. D. 1978, *Ap. J.*, **222**, 29.
Mathews, W. G., and Bregman, J. N. 1978, *Ap. J.*, **224**, 308.
Miller, L. 1986, *M.N.R.A.S.*, **220**, 713.
Norgaard-Nielsen, H. U., Jorgensen, H. E., and Hansen, L. 1984, *Astr. Ap.*, **135**, L3.
Ruppel, H. M., and Cloutman, L. D. 1975, *Los Alamos Nat. Rept.*, LA-6149-MS.
Sarazin, C. S. 1986, *Rev. Mod. Phys.*, **58**, 1.
———. 1987, in *Dark Matter in the Universe*, ed. J. Kormandy and G. P. Knapp (Dordrecht: Reidel), p. 183.
Silk, J., Djorgovski, S., Wise, R. F. G., and Bruzual, G. 1986, *Ap. J.*, **307**, 415.
Soker, N., and Sarazin, C. S. 1988, in *Proc. Workshop on Cooling Flows in Clusters and Galaxies*, ed. A. C. Fabian (Cambridge: Cambridge University Press), p. 367.
Spitzer, L. 1978, *Physical Processes in the Interstellar Medium* (New York: Wiley).
Tucker, W. H., and Rosner, R. 1983, *Ap. J.*, **267**, 547.

JOEL N. BREGMAN: National Radio Astronomy Observatory, Edgemont Road, Charlottesville, VA 22903

LAURENCE P. DAVID: Harvard-Smithsonian Center for Astrophysics, 60 Garden Street, Cambridge, MA 02138